



Characterization of the novel heterozygous *SCN5A* genetic variant Y739D associated with Brugada syndrome

Anastasia K. Zaytseva^{a,b,*}, Artem M. Kiselev^{a,c}, Alexander S. Boitsov^a, Yulia V. Fomicheva^a, Georgii S. Pavlov^a, Boris S. Zhorov^{a,b,d}, Anna A. Kostareva^{a,e}

^a Almazov National Medical Research Centre, St. Petersburg, 197341, Russia

^b Sechenov Institute of Evolutionary Physiology & Biochemistry, Russian Academy of Sciences, St. Petersburg, 194223, Russia

^c Institute of Cytology, Russian Academy of Sciences, Saint Petersburg, Russia

^d Department of Biochemistry and Biomedical Sciences, McMaster University, Hamilton, L8S 4K1, Canada

^e Department of Woman and Child Health, Karolinska Institute, Stockholm, 17176, Sweden

ARTICLE INFO

Keywords:

Brugada syndrome
Sodium channel
SCN5A
Sodium channelopathies
Homology modeling

ABSTRACT

Genetic variants in *SCN5A* gene were identified in patients with various arrhythmogenic conditions including Brugada syndrome. Despite significant progress of last decades in studying the molecular mechanism of arrhythmia-associated *SCN5A* mutations, the understanding of relationship between genetics, electrophysiological consequences and clinical phenotype is lacking. We have found a novel genetic variant Y739D in the *SCN5A*-encoded sodium channel $Na_v1.5$ of a male patient with Brugada syndrome (BrS). The objective of the study was to characterize the biophysical properties of $Na_v1.5$ -Y739D and provide possible explanation of the phenotype observed in the patient. The WT and Y739D channels were heterologously expressed in the HEK-293T cells and the whole-cell sodium currents were recorded. Substitution Y739D reduced the sodium current density by $47 \pm 2\%$ at -20 mV, positively shifted voltage-dependent activation, accelerated both fast and slow inactivation, and decelerated recovery from the slow inactivation. The Y739D loss-of-function phenotype likely causes the BrS manifestation. In the $hNa_v1.5$ homology models, which are based on the cryo-EM structure of rat $Na_v1.5$ channel, Y739 in the extracellular loop IIS1-S2 forms H-bonds with K1381 and E1435 and pi-cation contacts with K1397 (all in loop IIIS5-P1). In contrast, Y739D accepts H-bonds from K1397 and Y1434. Substantially different contacts of Y739 and Y739D with loop IIIS5-P1 would differently transmit allosteric signals from VSD-II to the fast-inactivation gate at the N-end of helix IIIS5 and slow-inactivation gate at the C-end of helix IIIP1. This may underlie the atomic mechanism of the Y739D channel dysfunction.

1. Introduction

Cardiac voltage-gated sodium channels ($Na_v1.5$) are responsible for the rapid inflow of sodium ions to cardiomyocytes during phase 0 of the action potential [1]. Genetic variants in the *SCN5A* gene, which encodes the pore-forming alpha subunit $Na_v1.5$, have been reported in patients with various arrhythmogenic disorders, including congenital long QT syndrome (LQT3), Brugada syndrome (BrS1), progressive cardiac conduction disease (PCCD), arrhythmogenic right ventricular cardiomyopathy (ARVC) and dilated cardiomyopathy (DCM) [1–3].

BrS is a rare congenital arrhythmic disorder with clinical manifestation varying from asymptomatic to sudden cardiac death [4]. BrS-associated genes include genes encoding sodium and calcium channels, as well as proteins affecting channel kinetics and trafficking [5]. It was shown that patients carrying *SCN5A* mutations have more pronounced epicardial electrical abnormalities and a more aggressive clinical presentation [6]. Moreover, the use of general anesthesia (single-bolus propofol and volatile anaesthetics) during ablation did not affect the prognostic value [7].

According to the ClinVar database, more than 900 missense genetic

Abbreviations: BrS, Brugada syndrome; Na_v , Voltage gated sodium channels; I_{Na} , Sodium current; VSD, Voltage-Sensing Domain; rNav1.5, rat Nav1.5; hNav1.5, human Nav1.5; P-loops, Membrane-diving extracellular loops between helices S5 and S6; P1 and P2, P-loop helices N- and C-terminal, respectively, to the selectivity filter residues; MC, Monte Carlo; MCM, MC-minimization; S1-S6, transmembrane helices in Nav1.5.

* Corresponding author. Almazov National Medical Research Centre, St. Petersburg, 197341, Russia.

E-mail address: zaytseva_ak@almazovcentre.ru (A.K. Zaytseva).

<https://doi.org/10.1016/j.bbrep.2022.101249>

Received 1 December 2021; Received in revised form 25 February 2022; Accepted 7 March 2022

2405-5808/© 2022 Published by Elsevier B.V. This is an open access article under the CC BY-NC-ND license (<http://creativecommons.org/licenses/by-nc-nd/4.0/>).

variants in *SCN5A* gene are associated with BrS, and most of them (more than 600) is classified as the variants of unknown significance. Less than 20% of known mutations were explored in heterologously expression system or in the models with endogeneous expression of mutant *SCN5A* forms such as iPSC, obtained from *SCN5A* variants carriers. The majority of biophysically characterized *SCN5A* genetic variants found in BrS patients demonstrated loss-of-function phenotype via various mechanisms. These include decreased surface density of the channels, altered voltage- and time-dependent activation/inactivation, and decelerated recovery from inactivation [8]. The alpha-subunit of $\text{Na}_v1.5$ contains four homologous repeats (I-IV). Each repeat has six transmembrane alpha-helical segments connected by extracellular and intracellular loops [9]. Segments S1-S4 in each repeat form a voltage-sensing domain (VSD), while helices S5 and S6 contribute to the pore domain. Here we report a novel genetic variant Y739D- $\text{Na}_v1.5$ found in a male patient with BrS. The objective of the study was to explore the biophysical consequences of new variant and suggest possible mechanisms, explaining our results. We generated *SCN5A*-Y739D, heterologously expressed it in the HEK293T expression system, and found that the genetic variant substantially changed biophysical characteristics of the Y739D vs. the WT channel. We observed reduction of sodium current density, depolarizing shift of steady-state activation, enhanced fast and slow inactivation, and decelerated recovery from the slow inactivation. A highly conserved tyrosine Y739 is located in the VSD-II extracellular loop IIS1-S2. We have built homology models of the $\text{hNa}_v1.5$ -WT and $\text{hNa}_v1.5$ -Y739D channels, compared intersegment contacts of Y739 and Y739D, and suggested possible mechanisms by which the genetic variant may affect activation and inactivation gating.

2. Results

2.1. Patient's phenotypic characterization and identification of the genetic variant

A 4-year-old male patient was diagnosed with Brugada syndrome based on typical ECG pattern manifesting during the fever episode – 38.4 °C during 4 h (Fig. 1A, B) and syncope anamnesis. No familial history of sudden cardiac death was registered in the family and none of the siblings revealed similar ECG-pattern or syncopies. Genetic analysis using a panel of 108 genes associated with cardiac inherited disorders revealed a novel *SCN5A* genetic variant Y739D (chr3: 38639267:A>C NM_001160161.2; c.2215T>G, p.Y739D) located in the extracellular loop IIS1-S2. None of the relatives carried the identified variant, thus it was considered to be *de novo* (Fig. 1C and D). This variant is not reported in gnomAD database, ClinVar or any other publicly available data bases, and was classified as pathogenic/damaging by most of the in silico prediction tools such as Mutation Tester, Mutation assessor, Provean, FIFT and LRT.

This variant is not reported in gnomAD database, ClinVar or any other databases. Based on ACMG guideline the variant was classified a variant of unknown significance. The variant was not identified neither in the parental nor in siblings, thus, being the most probably *de novo*.

2.2. Biophysical characterization of the $\text{Na}_v1.5$ -Y739D channel expressed in HEK293T cells

To elucidate the functional characteristics of the Y739D genetic variant we generated a plasmid vector with the corresponding substitution, expressed the *SCN5A*-WT or *SCN5A*-Y739D channels in the HEK293T cells, and recorded sodium currents (Fig. 2A, B). Mutant Y739D exhibited a typical sodium current, resembling that for the WT channel (Fig. 2C). The Y739D channel I_{Na} density measured at –20 mV from the holding potential of –100 mV was significantly smaller than that in WT (Fig. 2D, Table 1). We also observed in the genetic variant a mild depolarizing shift of the activation voltage-dependence and increased slope factor (Fig. 2E, Table 1). Thus, Y739D channels

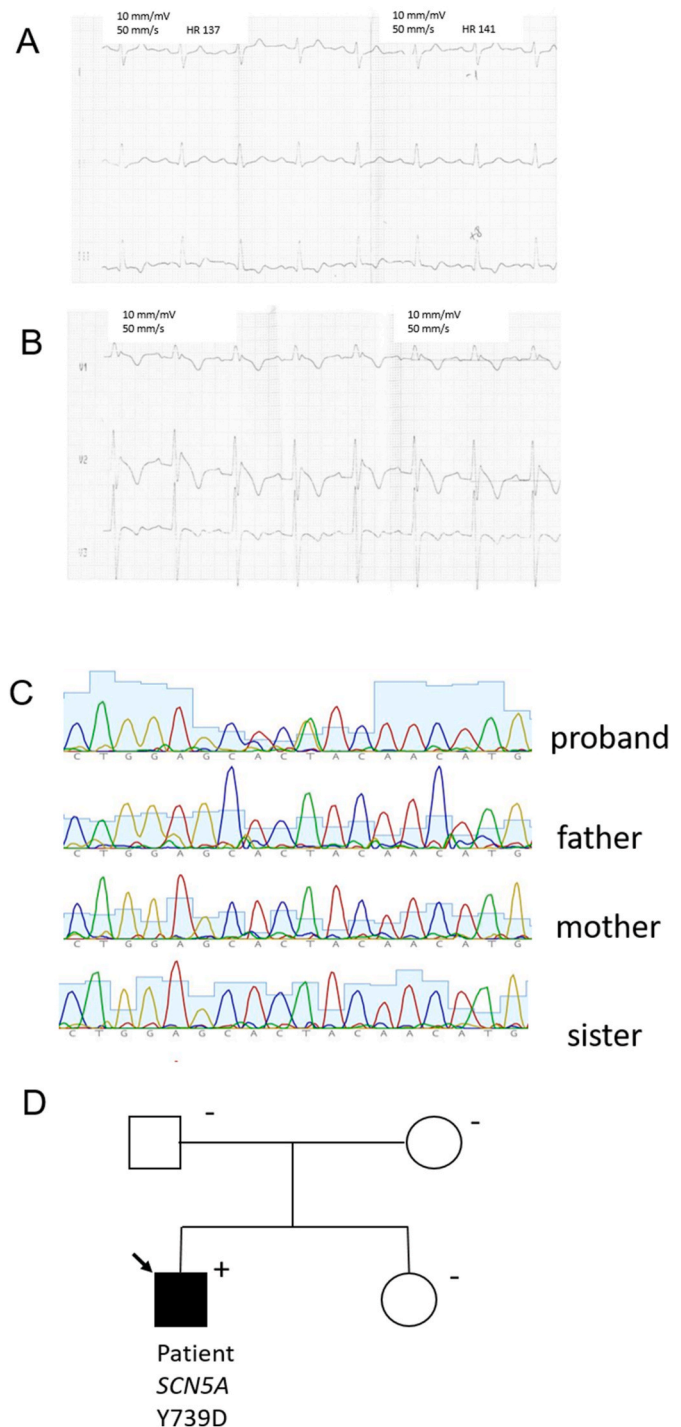


Fig. 1. A. ECG of the patient at normal temperature. B. ECG of the patient at fever. Fever lead to marked ST segment elevation. C. The pedigree of the proband. Parents and sister of the proband were unaffected. D. Results of Sanger sequencing of proband and his family.

activation requires more depolarizing potentials compare with that for WT channels.

To explore the impact of substitution Y739D on sodium channel function, we accessed the voltage-dependence of steady-state inactivation. We observed a negative shift of steady-state inactivation with no alterations in the slope factors (Fig. 3A, Table 1). However, this protocol did not allow us to distinguish whether the fast inactivation, slow inactivation or both were affected by Y739D. Therefore, we performed additional experiments and observed enhanced voltage-dependencies of

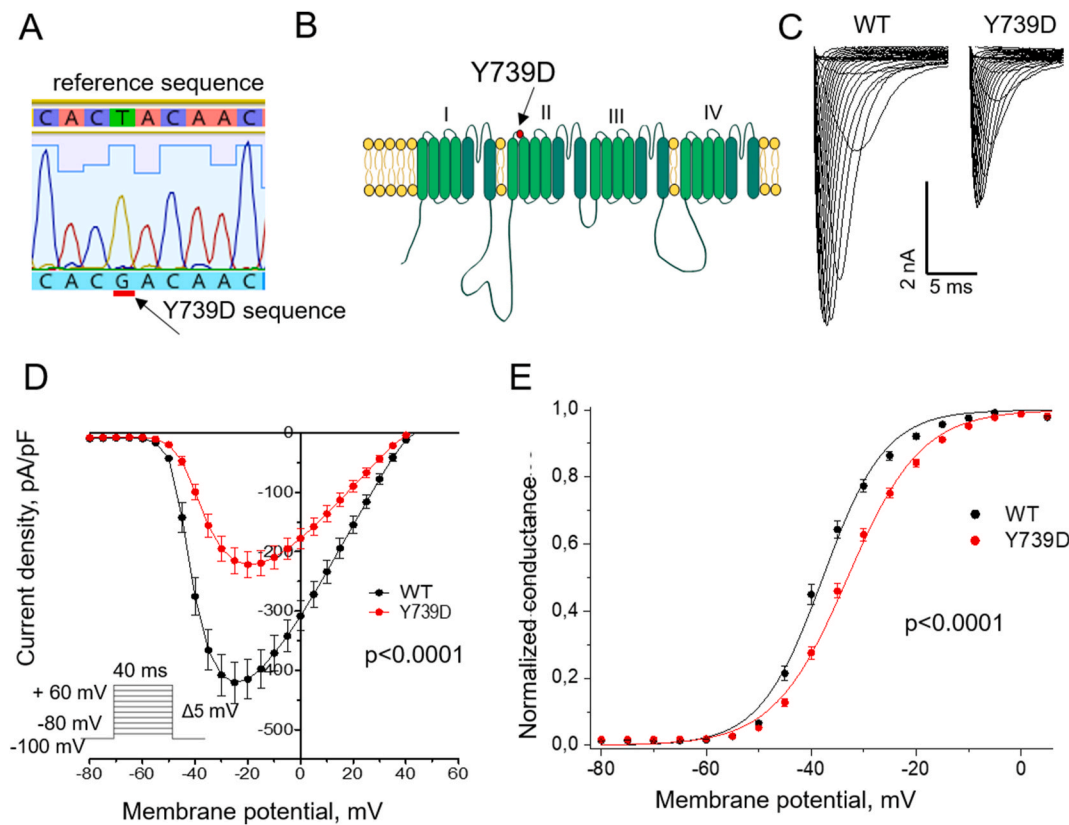


Fig. 2. Identification of novel genetic variant. A. Genetic characterization of the proband. Detail of the electropherograms obtained after *SCN5A* sequence analysis. The arrow indicates the nucleotide position 2209 in *SCN5A*, where the substitution (NM_198056.2:c.2209A<G, p.Y739D) was identified in the proband's DNA. B. Transmembrane topology of the Nav1.5 channel alpha-subunit. The arrow indicates position of the Y739D substitution in the S1-S2 loop of repeat domain II. C. Whole-cell current recordings of the WT and Y739D sodium channels. Representative sodium currents recorded from HEK293T cells expressing the channels are elicited by depolarizing steps from -80 mV to $+60$ mV in 10 mV increments from the holding potential of -100 mV. D. Current density-voltage relationship for WT (black circles, $N = 42$) and Y739D (black triangles, $N = 33$). E. The voltage dependence of activation for WT (black circles, $N = 42$) and Y739D (black triangles, $N = 33$). The solid lines show least-squares fits to the Boltzmann function for WT and Y739D.

both fast and slow inactivation (Fig. 3B and C, Table 1). Next, we analyzed the time courses of recovery from inactivation, fast inactivation and slow inactivation (Fig. 3D-F). The Y739D variant did not affect recovery from inactivation and fast inactivation, but impaired recovery from slow inactivation (Table 1).

We also found a significant change of the time constant of intermediate inactivation (Fig. 4A, Table 1), but no alterations in the onset kinetics of slow inactivation (Fig. 4B). We further analyzed activity-dependent loss of channel availability at various frequencies. A very small difference was found between WT and Y739D at the 5 Hz 100th pulse (WT: $94.6 \pm 1.9\%$, $n = 10$; Y739D: $88.8 \pm 3.0\%$, $n = 14$, $p = 0.135$) (Fig. 4C). In contrast, the Y739D I_{Na} evoked at the 10 Hz 100th pulse was significantly lower than that of WT (WT: $94.9 \pm 1.7\%$, $n = 8$; Y739D: $77.5 \pm 7.1\%$, $n = 6$, $p = 0.008$) (Fig. 4D). The normalized residual current levels recorded at the 0.66 Hz 30th pulse were $99.0 \pm 1.3\%$ for WT and $97 \pm 1.4\%$ for Y739D ($p = 0.26$) (Fig. 4E). The normalized residual current levels recorded at the 1.92 Hz 100th pulse were $44 \pm 4.2\%$ ($n = 8$) for WT and $27 \pm 2.7\%$ for Y739D ($n = 6$) (Fig. 4E).

2.3. Contacts of Y739 and Y739D in the rNav1.4-based models of hNav1.5

In the cryo-EM structure of the rNav_v1.5 channel [10], Y739 (hNav_v1.5 numbers) forms several contacts with the large extracellular loop IIIIS5-P1. These include H-bonds with salt-bridged K1381 and E1435, as well as pi-cation interaction with K1397, which does not form other strong contacts (Fig. 5 A). Similar contacts are seen in the Monte

Carlo-minimized model of hNav_v1.5. In the Monte Carlo-minimized model of hNav_v1.5_Y739D, aspartate D739 accepted an H-bond from Y1434 and formed a salt bridge with K1397 (Fig. 5B). Thus, substitution Y739D significantly changed contacts between extracellular loops in VSD-II (IIS1-S2) and the pore domain (IIIS5-P1).

3. Discussion

Brugada syndrome is a rare inherited cardiac disorder. According to the recent meta-analysis the worldwide pooled prevalence of BrS is 0.5 per 1000 [11]. The hallmark of BrS is the ST-segment elevation in the right precordial leads V1-V3 and right bundle branch block [4]. BrS is responsible for 20% of all sudden cardiac death cases without structural myocardial abnormalities [12]. This syndrome is associated with genetic variants in proteins, which control ionic balance in cardiomyocytes. These proteins are encoded by *SCN5A*, *GPD1L1*, *CACNA1C*, *KCNE3*, *SCN3B* and other genes [4]. The majority of genetic variants observed in patients with BrS are detected in gene *SCN5A*. Despite intense studies of biophysical mechanisms of arrhythmias, still less than a half of genetic variants described in patients with BrS are functionally characterized.

Here we reported a novel *SCN5A* genetic variant in a male patient with BrS. According to American College of Medical Genetics guidelines this variant is classified as variant of unknown significance. Sodium current in HEK293T cells with expressed Nav_v1.5_Y739D had several abnormalities: decreased peak current density, impaired activation and enhanced inactivation. In particular, variant Y739D negatively shifted steady-state inactivation and fast steady-state inactivation. It also accelerated intermediate inactivation and slow inactivation. If mutated

Table 1
Biophysical characteristics of Y739D channels.

		WT	n	Y739D	n	p
Current density at -20mV	pA/pF	-415.0 ± 33.8	42	-221.8 ± 22.1	33	<0.0001
Steady-state activation	$V_{1/2}$, mV	-37.8 ± 0.6	42	-33.1 ± 0.6	33	<0.0001
	k	5.3 ± 0.2		6.7 ± 0.2		<0.0001
Steady-state inactivation	$V_{1/2}$, mV	-82.3 ± 1.3	18	-86.9 ± 1.0	21	0.0335
	k	5.8 ± 0.2		5.9 ± 0.15		0.5
Steady-state fast inactivation	$V_{1/2}$, mV	-62.6 ± 1.3	10	-68.9 ± 1.4	15	0.0045
	k	9.0 ± 0.4		10.6 ± 0.3		0.0052
Recovery from fast inactivation	τ , ms	17.32 ± 2.07	11	24.35 ± 5.68	8	0.65
Recovery from inactivation	τ_{fast} , ms	16.5 ± 1.5	24	23.2 ± 5.5	9	0.73
	A_{fast}	0.89 ± 0.03		0.91 ± 0.06		0.5
	τ_{slow} , ms	227.0 ± 28.6		548.7 ± 289.3		0.27
	A_{slow}	0.21 ± 0.02		0.17 ± 0.04		0.28
Recovery from intermediate inactivation	τ_{fast} , ms	10.5 ± 0.9	15	18.1 ± 3.6	9	0.043
	A_{fast}	0.86 ± 0.018		0.79 ± 0.06		0.55
	τ_{slow} , ms	133.9 ± 12.5		172.7 ± 29.3		0.438
	A_{slow}	0.21 ± 0.016		0.24 ± 0.05		0.9
Onset of intermediate inactivation	τ , ms	1851.0 ± 175.8	8	1085.1 ± 254.5	6	0.042
	A	0.32 ± 0.05		0.37 ± 0.05		0.35

channel develops a slow inactivation at the time scale of fast inactivation of the WT channel, the shift of steady-state fast inactivation will be observed [13]. Therefore, we consider the slow inactivation enhancement as the major mechanism of Y739D-dependent development of BrS. Finally, we observed a slower recovery of $Na_v1.5$ -Y739D from the slow inactivation and significant decrease in activity-dependent loss of channel availability at certain frequencies. Thus, the decreased peak current density and changes in the Y739D channel gating can be due to altered $Na_v1.5$ kinetics rather than abnormalities in the channel trafficking. In summary, $Na_v1.5$ -Y739D demonstrated loss-of-function phenotype, which is consistent with our understanding of the BrS1 molecular mechanisms.

In the cryo-EM structure of $rNa_v1.5$, Y739 (hNav1.5 numbers) forms H-bonds with K1381 and E1435 and pi-cation contacts with K1397 (Fig. 5A). The latter also donates an H-bond to the backbone carbonyl of G1358 at the C-end of IIS5 (not shown for clarity). Very similar contacts between loops IIS1-S2 and IIS5-P1 are seen in the $rNa_v1.5$ -based model of hNav1.5. In the hNav1.5_Y739D model, Y739D accepts H-bonds from K1397 and Y1434 (Fig. 5B), while H-bond of K1397 with G1358 is lost. Substantially different contacts of Y739 and Y739D with loop III_S5-P1 would differently transmit allosteric signals from VSD-II in two directions. The first direction is through IIS5 towards the fast-inactivation tripeptide IFM (Fig. 5B), whose phenylalanine forms tight contacts with V1323 and A1326 at the N-end of IIS5. The second direction is through helix IIP1 towards K1419 in the selectivity-filter region (Fig. 5B), where the slow inactivation gate is located.

Y739 is conserved within $Na_v1.5$ paralogs and orthologs, indicating that tyrosine is essential at this position. According to the ClinVar database, loop II_S1-S2 and surrounding amino acids represent a hot spot for BrS-associated genetic variants A735E, A735V, A735T, L736P, H738P and E746K [14]. Moreover, the important role of S1-S2 loops in the channel functioning is consistent with the fact that mutation T353I

in I_S1-S2, identified in patients with BrS results in current density reduction and left shift of steady-state inactivation [15].

Substitutions that affect kinetics of slow inactivation were identified in different parts of the channel, indicating that multiple intersegment contacts are involved in this process. The impact of BrS-associated genetic variants on the transition to the slow inactivated state is described for only few substitutions. Respective studies report the enhancement of slow inactivation for mutations located in the C-terminal domain (D1595 N [16], R1629Q [17], Y1795H [18]), in the pore domain (G298S [16], D1714G [19]) and in the linker between transmembrane segments (G1319V [20]). Previously, we reported genetic variant A1294G in the extracellular loop IIS3-S4, which was found in our patient with combined phenotype, and found that the mutations enhanced slow inactivation [21]. Here we demonstrated that the IIS1-S2 loop is also involved in the process of slow inactivation.

In conclusion, here we have found a new *SCN5A* genetic variant Y739D in a patient with BrS1 and demonstrated that the loss-of-function of $Na_v1.5$ -Y739D expressed in HEK293T cells is due to accelerated slow and fast inactivation. In homology models of the WT and mutated channels, extracellular loops IIS1-S2 in VSD-II and IIS5-P1 in the pore domain have substantially different contacts. The models suggest that helices IIS5 and IIP1 are involved in the allosteric signal transduction from VSD-II to the fast and slow inactivation gates, respectively.

4. Methods

4.1. Clinical data

The study was performed according to the Declaration of Helsinki. Approval was obtained from the Almazov National Medical Research Centre Ethical Committee. Written consent was obtained from the patient prior to investigation.

4.2. Genetic analysis, mutagenesis and heterologous expression

Target sequencing was performed on Illumina MiSeq using Haloplex enrichment kit with a panel of 108 genes associated with inherited cardiac disorders as previously described [22]. All disease-related genetic variants were confirmed by Sanger sequencing and classified according to American College of Medical Genetics guidelines [23].

The pcDNA3.1 vector with WT hNav1.5 and GFP (hH1-pcDNA3.1) was kindly provided by Prof. Hugues Abriel (Institute of Biochemistry and Molecular Medicine, University of Bern, Bern, Switzerland). Site-directed mutagenesis was performed by the PCR amplification according to standard mutagenesis protocol with overlapped primers (TGTGTGCTGCTCCAGCGCCATGAAGAGTGT; TGGAGCAGCACAA-CATGACAAGTGAATTTCG). hH1-pcDNA3.1 (1 μ g) or Y739D-pcDNA3.1 (1 μ g) were transfected into HEK293T cells growing on 3-cm plates using 1 mg/ml water solution of linear polyethylenimine hydrochloride (PEI, MW 40,000, Polysciences) at 2:1 v/w ratio with pDNA. The cells were maintained in the DMEM medium supplement 2 mM glutamine, 100 U/ml penicillin, 100 μ g/ml streptomycin (Thermo Fisher Scientific) in a CO₂ incubator at +37 °C for 24 h and then seeded at poly-Lysine (Sigma Aldrich) coated glasses for electrophysiological recordings.

4.3. Electrophysiology

Sodium current (I_{Na}) was recorded using patch-clamp method (whole-cell configuration). All measurements were performed at room temperature. The extracellular solution contained (mmol/L): 140 NaCl, 1 MgCl₂, 1.8 CaCl₂, 10 HEPES, 10 Glucose (pH 7.4 CsOH). The intracellular solution contained (mmol/L): 130 CsCl, 10NaCl, 10 EGTA, 10 HEPES (pH 7.3 CsOH). Microelectrodes were manufactured from the borosilicate glass using a puller (P-1000, Sutter Instrument). The electrode resistance varied from 1.8 to 2.5 M Ω . The series resistance was compensated at 75–80%. Data acquisition was performed using

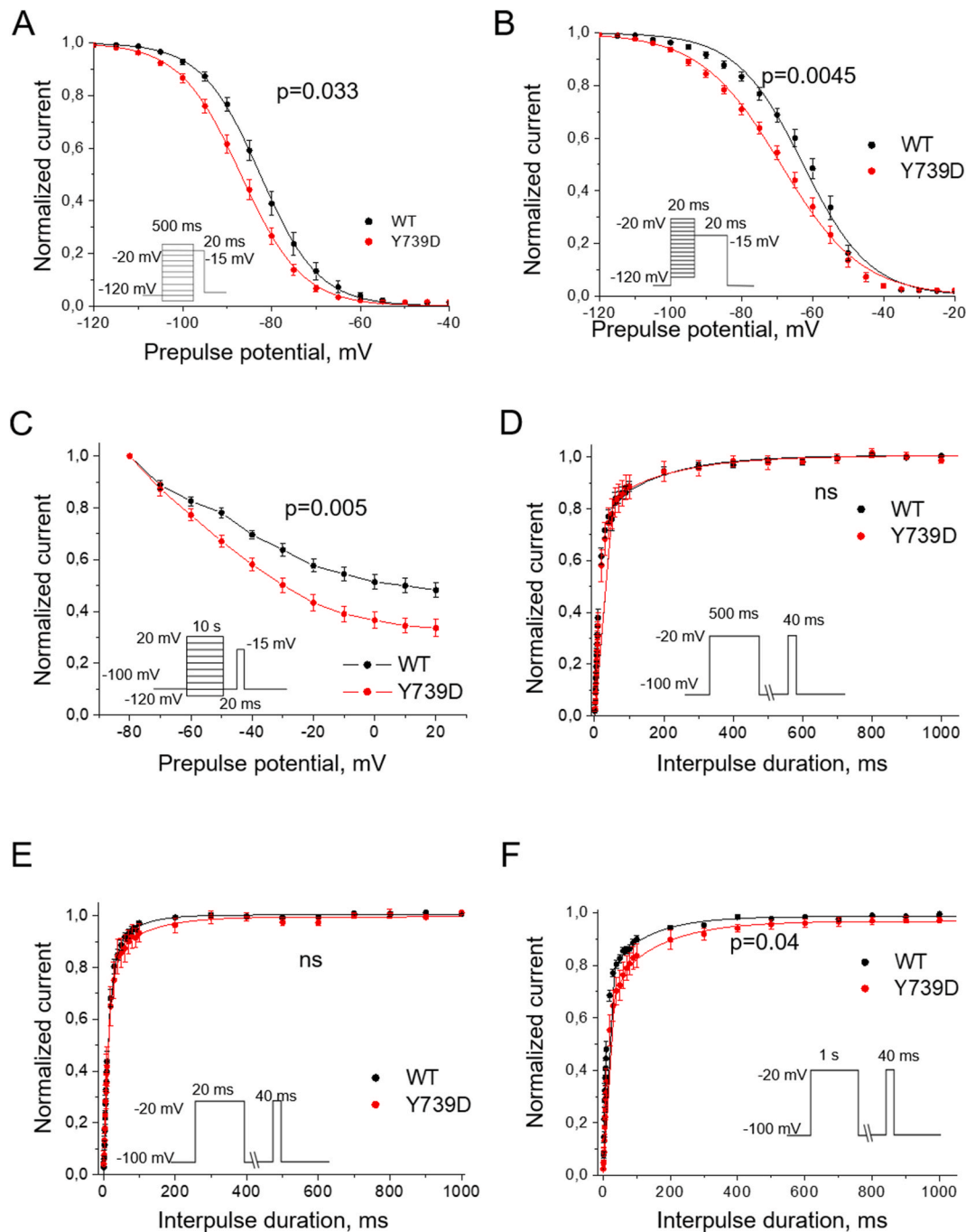


Fig. 3. A. The voltage-dependence of steady-state inactivation. Solid lines show least-square fits to the Boltzmann function for WT and Y739D. B. The voltage-dependence of steady-state fast inactivation. C. The voltage-dependence of steady-state slow inactivation. Y739D channels demonstrated enhanced slow inactivation vs. WT ($I_{Na}/I_{Na_{max}}$ at +20 mV WT: 0.48 ± 0.03 , $N = 12$; Y739D: 0.33 ± 0.03 , $N = 15$, $p = 0.005$). D. The time course of recovery from inactivation for WT (black circles, $N = 24$) and Y739D (black triangles, $N = 9$). E. The time course of recovery from fast inactivation for WT (black circles, $N = 13$) and Y739D (black triangles, $N = 10$). F. The time course of recovery from slow inactivation for WT (black circles, $N = 13$) and Y739D (black triangles, $N = 10$).

amplifier Axopatch 200B (Molecular devices). Currents were acquired at 20–50 kHz and low-pass filtered at 5 kHz using an analog-to-digital interface (Digidata 1440A acquisition system, Molecular devices). At least 3 independent transfections were used for electrophysiological recordings. N means number of cells.

4.4. Data analysis

The holding potential was -100 mV. Current-voltage (I - V) curves were recorded using protocol with depolarizing voltage steps from -80

to 60 mV during 40 ms in 5 mV steps at 1 Hz frequency. Peak I_{Na} at each voltage (V) was measured and corresponding conductance (G) was calculated by using equation: $G = I_{Na}/(V - V_{rev})$. Normalized conductance was plotted against voltage and G - V curves reflecting voltage-dependence of steady-state activation. These data were fitted to the Boltzmann function: $G/G_{max} = 1/(1 + \exp((V_{1/2} - V)/k))$, where G_{max} is the maximal sodium conductance, $V_{1/2}$ is the potential of half-maximal activation, and k is the slope factor. Current densities at each test potential were assessed by dividing I_{Na} by the cell capacitance.

Voltage-dependency of steady-state inactivation was obtained by

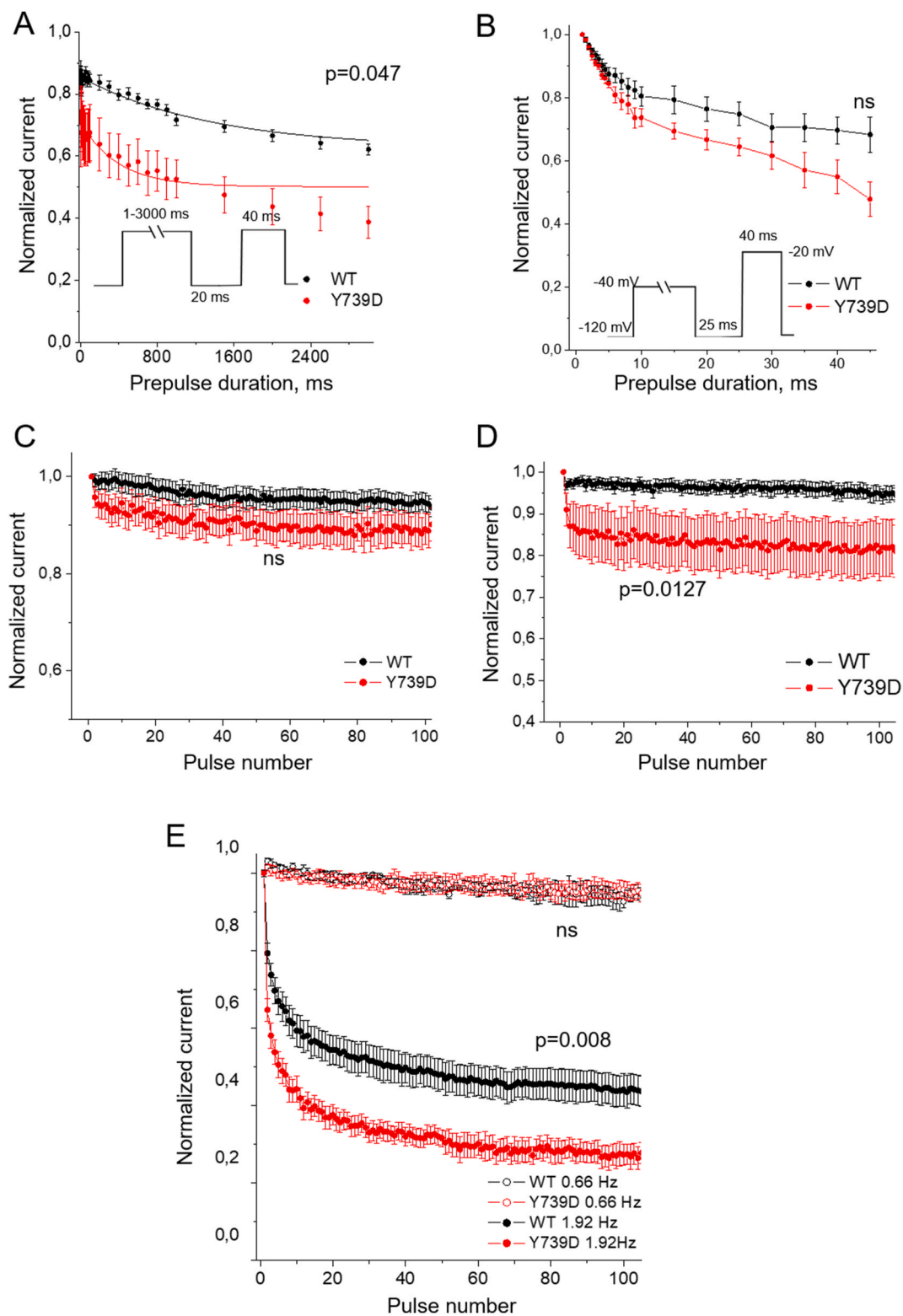


Fig. 4. A. The time course of onset of intermediate inactivation. Solid lines show least-squares fits to the mono-exponential function. B. Onset of the slow inactivation for WT (circles, N = 16) and Y739D (triangles, N = 10). Slow inactivation of the Y739D channel remained unchanged vs. WT ($p = 0.44$ for 45s). C. The normalized residual current levels at 5 Hz for WT (circles) and Y739D (triangles). D. The normalized residual current levels at 10 Hz for WT (circles) and Y739D (triangles). E. The normalized residual current levels recorded at 0.66 Hz for WT (open circles) and Y739D (open triangles) and at 1.92 Hz for WT (filled circles) and Y739D (filled triangles).

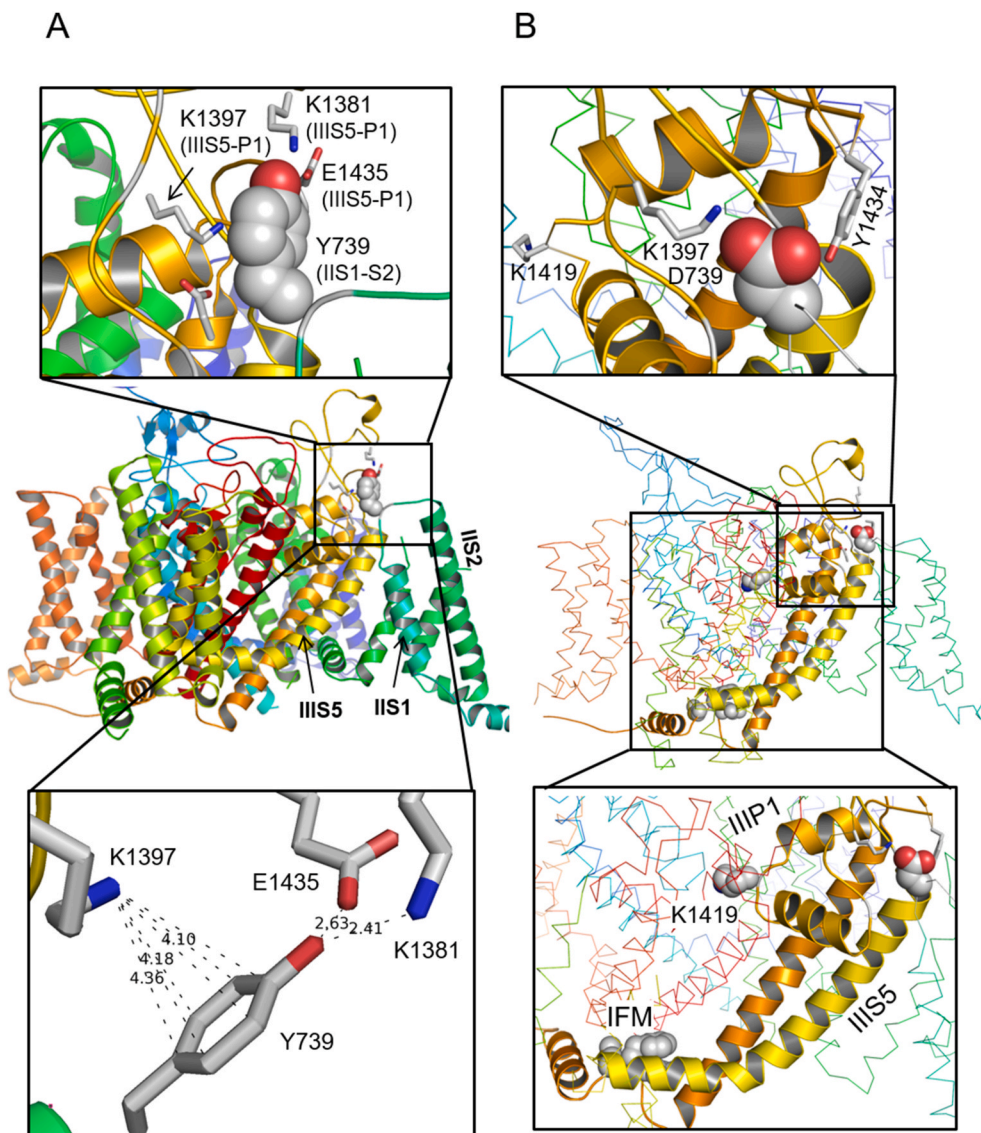


Fig. 5. A, In the cryo-EM structure of the rNav1.5 channel, Y739 forms H-bonds with K1381 and E1435 and a pi-cation contact with K1397 (Residue numbers correspond to hNav1.5). The latter also donates an H-bond to the backbone carbonyl of G1358 at the C-end of IIIS5 (not shown for clarity). B, In the model of hNav1.5_Y739D, Y739D accepts H-bonds from K1397 and Y1434, whereas the H-bond of K1397 with the backbone carbonyl G1358 is lost. Substantially different contacts of Y739 and Y739D with loop IIIS5-P1 would differently transduce allosteric signals from VSD-II through IIIS5 towards the fast-inactivation tripeptide IFM, and through IIIP1 towards lysine K1418 in the selectivity-filter region where the slow inactivation gate is located.

using two-step protocol with 500 ms prepulse varying from -120 to 0 mV with 5 mV increments and testing 20 ms step to -15 mV. Normalized testing I_{Na} was plotted against the prepulse voltage. Steady-state inactivation curves were fitted with the Boltzmann function. Voltage-dependency of fast inactivation was evaluated in similar way, but duration of the varying prepulse was 20 ms. Voltage-dependency of steady-state slow inactivation data were recorded using 10 s prepulse followed by a 20 ms hyperpolarization to -100 mV to allow recovery from fast inactivation.

The time course of recovery from inactivation was obtained using two-step protocol. First conditioning pulse lasts 500 ms at -15 mV followed by a recovering hyperpolarization gap at -100 mV, which duration varying from 1 to 3000 ms (recovery time) and 20 ms test pulse at -15 mV. I_{Na} recorded from the test pulse was normalized to that from the first conditioning pulse and plotted against the recovery time. Curves were fitted with the double-exponential function:

$$y = A_{fast} \times (1 - \exp(-t/\tau_{fast})) + A_{slow} \times (1 - \exp(-t/\tau_{slow}))$$

where A_{fast} and A_{slow} are fractions of the fast and slow inactivating components, respectively, and τ_{fast} and τ_{slow} are their time constants. The time course of recovery from fast and intermediate inactivation were accessed using the same protocol, but with 20 ms and 1 s prepulse

duration, respectively.

The development of intermediate inactivation was evaluated using double-pulse protocol. First step at -15 mV with duration from 1 to 3000 ms followed by 20 ms of hyperpolarization gap at -100 mV and second test step at -15 mV. I_{Na} elicited from the testing step was normalized to that from the first step and plotted against the duration of the first step. Curves were fitted with the mono-exponential function: $y = y_0 + A \times \exp(-t/\tau)$, where τ is the time constant. The development of slow inactivation was assessed using double-pulse protocol with varying duration (1 – 45 s) of the first step to -40 mV (P1) and testing step of 40 ms to -15 mV. I_{Na} elicited from the second test pulse at -15 mV was normalized to that from the first conditioning step and plotted against the first step duration.

Activity-dependent loss of channel availability was measured by applying repetitive depolarizing pulses to -15 mV at different frequencies (50 ms pulses at 5 Hz, 25 ms pulses at 10 Hz and 500 ms pulses at 0.66 Hz and 1.92 Hz). I_{Na} evoked by each pulse was normalized to the current induced by the first pulse.

4.5. Statistical analysis

All data are expressed as the mean values and standard errors (SEM). Statistical comparisons were made using the unpaired Mann-Whitney

test with $p < 0.05$ considered to be statistically significant. In some Figures, the standard error bars are smaller than the data symbols.

4.6. Homology modeling

Cryo-EM structure of the rat Na_v1.5 channel [10] and ZMM program [24] were used to build homology models of hNa_v1.5 and hNa_v1.4_Y739D. The models were Monte Carlo-minimized as described elsewhere [25]. In the Cryo-EM template many side chains are not resolved. Upon Monte Carlo minimization all residues adopted energetically optimal conformations, while the mainchain conformations remained practically the same as in the template.

Declaration of interests

The authors declare that they have no known competing financial interests or personal relationships that could have appeared to influence the work reported in this paper.

Data availability

Data will be made available on request.

Acknowledgements

This research was funded by the Ministry of Science and Higher Education of the Russian Federation (Agreement No. 075-15-2020-901). Homology modeling was performed using facilities of Compute Canada (www.compute-canada.ca).

Appendix A. Supplementary data

Supplementary data to this article can be found online at <https://doi.org/10.1016/j.bbrep.2022.101249>.

References

- [1] A.S. Amin, A. Asghari-Roodsari, H.L. Tan, Cardiac sodium channelopathies, *Pflügers Archiv* 460 (2010) 223–237, <https://doi.org/10.1007/s00424-009-0761-0>.
- [2] J.D. Kapplinger, D.J. Tester, M. Alders, B. Benito, M. Berthet, J. Brugada, P. Brugada, V. Fressart, A. Guerschicoff, C. Harris-Kerr, et al., An international compendium of mutations in the SCN5A-encoded cardiac sodium channel in patients referred for Brugada syndrome genetic testing, *Heart Rhythm* 7 (2010) 33–46, <https://doi.org/10.1016/j.hrthm.2009.09.069>.
- [3] P. Brugada, Brugada syndrome: more than 20 years of scientific excitement, *J. Cardiol.* 67 (2016) 215–220, <https://doi.org/10.1016/j.jcc.2015.08.009>.
- [4] G. Coppola, E. Corrado, A. Curnis, G. Maglia, D. Oriente, A. Mignano, P. Brugada, Update on Brugada syndrome 2019, *Curr. Probl. Cardiol.* (2019) 100454, <https://doi.org/10.1016/j.cpcardiol.2019.100454>, 10.1016/j.cpcardiol.2019.100454.
- [5] H. Watanabe, T. Minamino, Genetics of Brugada syndrome, *J. Hum. Genet.* 61 (2016) 57–60, <https://doi.org/10.1038/jhg.2015.97>.
- [6] G. Ciconte, M.M. Monasky, V. Santinelli, E. Micaglio, G. Vicedomini, L. Anastasia, G. Negro, V. Borrelli, L. Giannelli, F. Santini, et al., Brugada syndrome genetics is associated with phenotype severity, *Eur. Heart J.* 42 (2021) 1082–1090, <https://doi.org/10.1093/eurheartj/ehaa942>.
- [7] C. Pappone, G. Ciconte, E. Micaglio, M.M. Monasky, Common modulators of Brugada syndrome phenotype do not affect SCN5A prognostic value, *Eur. Heart J.* 42 (2021) 1273–1274, <https://doi.org/10.1093/eurheartj/ehab071>.
- [8] E. Savio-Galimberti, M. Argenziano, C. Antzelevitch, Cardiac arrhythmias related to sodium channel dysfunction, *Handb. Exp. Pharmacol.* 246 (2018) 331–354, https://doi.org/10.1007/164_2017_43.
- [9] W.A. Catterall, Voltage-gated sodium channels at 60: structure, function and pathophysiology, *J. Physiol.* 590 (2012) 2577–2589, <https://doi.org/10.1113/jphysiol.2011.224204>.
- [10] D. Jiang, H. Shi, L. Tonggu, T.M. Gamal El-Din, M.J. Linares, Y. Zhao, C. Yoshioka, N. Zheng, W.A. Catterall, Structure of the cardiac sodium channel, *Cell* 180 (2020) 122–134 e110, <https://doi.org/10.1016/j.cell.2019.11.041>.
- [11] W. Vutthikraivit, P. Rattanawong, P. Putthapiban, W. Sukhumthamarat, P. Vathesatogkit, T. Ngarmukos, A. Thakkinstian, Worldwide prevalence of Brugada syndrome: a systematic review and meta-analysis, *Acta Cardiol. Sin.* 34 (2018) 267–277, [https://doi.org/10.6515/acs.201805.34\(3\).20180302b](https://doi.org/10.6515/acs.201805.34(3).20180302b).
- [12] B. Benito, J. Brugada, R. Brugada, P. Brugada, Brugada syndrome, *Rev. Esp. Cardiol.* 62 (2009) 1297–1315, [https://doi.org/10.1016/s1885-5857\(09\)73357-2](https://doi.org/10.1016/s1885-5857(09)73357-2).
- [13] Y. Du, D.B. Tikhonov, Y. Nomura, K. Dong, B.S. Zhorov, Mutational analysis of state-dependent contacts in the pore module of eukaryotic sodium channels, *Arch. Biochem. Biophys.* 652 (2018) 59–70, <https://doi.org/10.1016/j.abb.2018.06.008>.
- [14] W. Huang, M. Liu, S.F. Yan, N. Yan, Structure-based assessment of disease-related mutations in human voltage-gated sodium channels, *Protein Cell* 8 (2017) 401–438, <https://doi.org/10.1007/s13238-017-0372-z>.
- [15] A.E. Pfahnl, P.C. Viswanathan, R. Weiss, L.L. Shang, S. Sanyal, V. Shusterman, C. Kornblit, B. London, S.C. Dudley Jr., A sodium channel pore mutation causing Brugada syndrome, *Heart Rhythm* 4 (2007) 46–53, <https://doi.org/10.1016/j.hrthm.2006.09.031>.
- [16] D.W. Wang, P.C. Viswanathan, J.R. Balsler, A.L. George Jr., D.W. Benson, Clinical, genetic, and biophysical characterization of SCN5A mutations associated with atrioventricular conduction block, *Circulation* 105 (2002) 341–346, <https://doi.org/10.1161/hc0302.102592>.
- [17] Z. Zeng, J. Zhou, Y. Hou, X. Liang, Z. Zhang, X. Xu, Q. Xie, W. Li, Z. Huang, Electrophysiological characteristics of a SCN5A voltage sensor mutation R1629Q associated with Brugada syndrome, *PLoS One* 8 (2013), e78382, <https://doi.org/10.1371/journal.pone.0078382>.
- [18] I. Rivolta, H. Abriel, M. Tateyama, H. Liu, M. Memmi, P. Vardas, C. Napolitano, S. G. Priori, R.S. Kass, Inherited Brugada and long QT-3 syndrome mutations of a single residue of the cardiac sodium channel confer distinct channel and clinical phenotypes, *J. Biol. Chem.* 276 (2001) 30623–30630, <https://doi.org/10.1074/jbc.M104471200>.
- [19] A.S. Amin, A.O. Verkerk, Z.A. Bhuiyan, A.A. Wilde, H.L. Tan, Novel Brugada syndrome-causing mutation in ion-conducting pore of cardiac Na⁺ channel does not affect ion selectivity properties, *Acta Physiol. Scand.* 185 (2005) 291–301, <https://doi.org/10.1111/j.1365-201X.2005.01496.x>.
- [20] S. Casini, H.L. Tan, Z.A. Bhuiyan, C.R. Bezzina, P. Barnett, E. Cerbai, A. Mugelli, A. A. Wilde, M.W. Veldkamp, Characterization of a novel SCN5A mutation associated with Brugada syndrome reveals involvement of DIIS4-S5 linker in slow inactivation, *Cardiovasc. Res.* 76 (2007) 418–429, <https://doi.org/10.1016/j.cardiores.2007.08.005>.
- [21] A.K. Zaytseva, A.V. Karpushev, A.M. Kiselev, E.N. Mikhaylov, D.S. Lebedev, B. S. Zhorov, A.A. Kostareva, Characterization of a novel SCN5A genetic variant A1294G associated with mixed clinical phenotype, *Biochem. Biophys. Res. Commun.* 516 (2019) 777–783, <https://doi.org/10.1016/j.bbrc.2019.06.080>.
- [22] A. Kostareva, A. Kiselev, A. Gudkova, G. Frishman, A. Ruepp, D. Frishman, N. Smolina, S. Tarnovskaya, D. Nilsson, A. Zlotina, et al., Genetic spectrum of idiopathic restrictive cardiomyopathy uncovered by next-generation sequencing, *PLoS One* 11 (2016), e0163362, <https://doi.org/10.1371/journal.pone.0163362>.
- [23] S. Richards, N. Aziz, S. Bale, D. Bick, S. Das, J. Gastier-Foster, W.W. Grody, M. Hegde, E. Lyon, E. Spector, et al., Standards and guidelines for the interpretation of sequence variants: a joint consensus recommendation of the American College of medical genetics and genomics and the association for molecular pathology, *Genet. Med.* 17 (2015) 405–424, <https://doi.org/10.1038/gim.2015.30>.
- [24] D.P. Garden, B.S. Zhorov, Docking flexible ligands in proteins with a solvent exposure- and distance-dependent dielectric function, *J. Comput. Aided Mol. Des.* 24 (2010) 91–105, <https://doi.org/10.1007/s10822-009-9317-9>.
- [25] V.S. Korkosh, B.S. Zhorov, D.B. Tikhonov, Folding similarity of the outer pore region in prokaryotic and eukaryotic sodium channels revealed by docking of conotoxins GIIIA, PIIIA, and KIIIA in a NavAb-based model of Nav1.4, *J. Gen. Physiol.* 144 (2014) 231–244, <https://doi.org/10.1085/jgp.201411226>.